Environmental Science Advances

ROYAL SOCIETY OF CHEMISTRY

PAPER

View Article Online
View Journal

Cite this: DOI: 10.1039/d6va00121a

Upcycling of PET-based plastic bottles into carbon dots for photocatalytic degradation of Reactive Black 5 using response surface methodology

Seemab Javed,[ad] Shahzad Ali Shahid Chatha,*[a] Shafqat Ali[bc] and Aman Ullah *[d]

Water contamination and plastic pollution are the most prominent environmental issues, demanding state-of-the-art, sustainable remediation strategies. This study describes the upcycling of waste polyethylene terephthalate (PET) bottles into carbon dots (CDs) and their application for the degradation of Reactive Black 5 (RB5) dye in water. CDs derived from PET were successfully synthesized through a multistep green approach. The synthesized CDs were characterized for their structural, optical and surface features. UV-Vis revealed typical CD absorption behavior with an optical band gap of 3.14 eV. pH-dependent fluorescence spectra confirmed the presence of surface-state emission. FTIR, XRD, DLS, and AFM results were consistent with the presence of surface functionalities and defects, surface-domains of disordered carbon materials, nanoparticle dispersion and CD-like morphology. Box–Behnken-based Response Surface Methodology (RSM) models were established and optimum conditions were found by studying the effects of important operational parameters on RB5 degradation. The synthesized CDs exhibit a high removal rate of RB5 under light illumination (79.6–91.2%), whereas dark removal was relatively low (10.7–18.4%), which indicates that the major contribution came through light-driven processes, with the net photocatalytic degradation being high (68.9–72.8%). The RSM study established a region of optimal operation (pH = 7.4, CD dose = 0.50 g L^{-1}, time = 75 minutes, and RB5 = 26 mg L^{-1}). The experimental response was very similar to the predicted one, and this confirms the accuracy of the statistical optimization. PET-derived CDs offer an inexpensive, green, and efficient medium for dye-contaminated wastewater purification.

Received 10th March 2026
Accepted 27th May 2026

DOI: 10.1039/d6va00121a

rsc.li/esadvances

Environmental significance

Increasing plastic waste and dye-contaminated wastewater are some of the major environmental issues. Upcycling of plastic waste into carbon dots for photocatalytic applications is a sustainable approach to waste management and water purification. This study upcycled waste PET bottles into functional carbon dots and employed them in the photocatalytic degradation process of Reactive Black 5 dye. The response surface methodology was used to determine the optimal operating conditions and increase degradation efficiency. The study also introduces a straightforward waste-to-value economic plan that can advance the circular economy objective and serve as a powerful method for treating dye-contaminated water.

1 Introduction

Plastic pollution and industrial wastewater are two prominent environmental challenges of the modern era, causing widespread pollution and driving climate change.[1,2] Currently available strategies to address plastic waste-related issues, including mechanical recycling, incineration, and landfilling, have been reported to have limitations.[3] Thus, the shortcomings of conventional techniques underscore the need to develop cutting-edge upcycling technologies to transform discarded plastic components into valuable, novel materials. Recently, various research studies have attempted to transform discarded polymeric components into valuable carbon nanomaterials, such as graphene, carbon nanotubes, and carbon quantum dots.[4] Unlike mixed or composite plastics, the consistent chemical structure of PET, in which repeating units of terephthalate and ethylene glycol are linked, and its high carbon content make it an ideal candidate for transformation into valuable carbon-based nanomaterials.[5] Its aromatic structure provides a strong foundation for forming graphitic networks of sp^2 hybridized carbon, while the polymer backbone contains oxygen groups that enhance the surface properties of the resulting carbon dots.[6–9] PET bottles can be converted into activated carbon for the degradation of Brilliant Green dye,

[a]Department of Chemistry, Government College University, Faisalabad-38000, Pakistan. E-mail: chatha222@gmail.com
[b]Department of Environmental Science, Government College University, Faisalabad-38000, Pakistan
[c]Department of Biological Sciences and Technology, China Medical University, Taichung 40402, Taiwan
[d]Department of Agricultural, Life & Environmental Sciences, University of Alberta, T6G 2G7, Canada. E-mail: ullah2@ualberta.ca

confirming the potential of plastic-waste-derived carbon dots in water treatment applications.[10] Carbon dots represent a distinct class of zero-dimensional carbon-based nanomaterials with diameters usually smaller than 10 nm. Remarkable features of these particles, like chemical stability, low toxicity and photoluminescence, make them attractive for multiple applications. In terms of structure, the particles comprise a graphitic structure with a large number of sp^2 bonds, together with surface groups containing oxygen atoms.[11,12] These characteristics make them excellent candidates for environmental applications, including metal removal, degradation of organic contaminants, and biosensing.[13] In parallel, textile wastes containing high levels of recalcitrant colorants pose significant health and ecological hazards and are not easily treatable.[14] One of the common reactive azo dyes is Reactive Black 5 (RB5), which is particularly recalcitrant due to its complex structure, aromaticity, and stability, necessitating a sustainable strategy for its removal from waterbodies.[15,16] Despite extensive research the existing dye-treatment methods are not up to the mark, as physical adsorption can relocate contaminants instead of destroying them and might produce secondary waste; biological treatment may be sluggish and susceptible to inhibitory effluent matrices, and chemical oxidation/coagulation may need a substantial number of reagents and strict pH control yet still result in incomplete mineralization of complex wastewater.[14] Photocatalysis is a promising approach; recent research has highlighted the need for environmentally friendly materials for the removal of dyes from wastewater. Effective photo-assisted degradation of wastewater dyes using CdS nanoparticles trapped in porous g-C_3N_4/SiO_2 composites shows the importance of engineered photocatalysts for the removal of organic dyes.[17] A calcium alginate–polydopamine biocomposite for sustainable removal of Brilliant Green dye indicates the growing interest in greener adsorbent systems for dye remediation.[18] Efficient photocatalytic systems are still largely developed with hybrid and chemical synthesis. Meanwhile, the conversion of urban and plastic waste is increasingly recognized as a key approach to sustainable environmental management, but further valorization strategies are needed to create functional materials.[19]

In this context, carbon dots (CDs) have become popular low-toxicity, tunable, and photostable nanomaterials, which can serve as photocatalysts, especially under visible light, to achieve water treatment in the real world.[20] Recent studies demonstrate that carbon-dot nanomaterials are promising in photo/electrocatalytic removal of organic pollutants, owing to their photoresponsive features, functionality and charge carrier transfer.[21] In this regard, this project upcycling plastic waste into carbon dots and their application for photocatalytic degradation of RB5 addresses problems in a single integrated process. This two-fold solution connects the plastic waste management with wastewater treatment directly, and takes advantage of the fact that CD semiconductor systems can be used to amplify light absorption and charge transfer to accelerate the degradation of dyes.[22] In photocatalysis, interacting variables are important to process performance; hence, Response Surface Methodology (RSM), particularly Box–Behnken Design (BBD), can be a good choice to model the nonlinear nature of process performance and determine the real optima with fewer experiments compared to one-factor-at-a-time tests.[23,24] Overall, this study focuses on the synthesis of plastic-based carbon dots, which can be regarded as a viable platform for the photocatalytic elimination of RB5 and RSM-BBD, thereby optimizing working conditions and achieving maximum degradation efficiency and feasibility. The most significant future directions are also expected to include performance validation on real textile wastewater across more water chemistries, catalyst recovery/reuse, and long-term photostability, performance, and integration into the optimized process in continuous-flow or sunlight-driven reactors.

2 Materials and methods

2.1 Chemicals and reagents

In this study, a sustainable approach was applied, and no harsh chemicals were used for the preparation. In the dye degradation study, only hydrochloric acid (HCl, analytical grade, Merck, Germany) and sodium hydroxide (NaOH, analytical grade, Sigma-Aldrich, USA) were used to adjust the pH.

2.2 Pre-treatment of polyethene terephthalate (PET) based plastic waste

Polyethene terephthalate (PET) waste bottles were collected from the cafeteria of Government College University, Faisalabad, Pakistan. Over a period of one month, discarded PET bottles were collected manually, illustrating the extensive consumption of bottled water and ensuring a continuous supply of PET waste. These bottles were sorted by color and labeling to minimize contamination risk. Only transparent PET bottles with specific colors and coatings were used to ensure contamination-free samples, as such features can affect the quality and composition of the carbon dots. The PET bottles were thoroughly cleaned and dried at room temperature, then washed with tap water, followed by distilled water, and finally dried to remove all soluble contaminants.[25] The bottles were then dried at room temperature and shredded into small pieces using a mechanical shredder. The shredded sample was dried at 60 0C for 12 hours in a heating oven (NR-38XDG, JW-Enviro) and stored in a polyethylene zipper bag for further experiments.

2.3 Synthesis of CDs

In the calcination stage, a starting material, 3.0 g of pre-treated PET, was poured into a ceramic crucible and heated in a muffle furnace (B-170 (Nabertherm) for 5 hours at 500 °C. Thermal treatment of PET results in carbonized material. After calcination, the carbonized PET is cooled to ambient temperature (25 °C) to avoid rapid structural changes from thermal shock. Then, 50 mL of deionized water is added to extract the carbon dots, thereby aiding their dispersion. The calcined product was a blackish-brown powder that was sieved through a 0.21 mm screen, and larger particles were removed using an electric mortar and pestle. The fine powder was added to a solution of distilled water and stirred thoroughly at room temperature for 24 hours under appropriate conditions. This stirring was used

to achieve uniform dispersion of carbon nanoparticles. Hydrothermal treatment at 180 °C was conducted in a sealed Teflon-lined autoclave for 6 hours. This process breaks down polymer chains into carbon-rich particles, converting the plastic into carbon dots, as previously reported.[25] The obtained crude carbon dot (CD) solutions were sonicated for 30 minutes for 100 W at 25 °C to ensure proper dispersion of any formed clumps. The purpose of sonication was not only to break up agglomerates but also to modify the surface functional groups of the CDs and facilitate dopant incorporation.[26] The yield of carbon dots was calculated using the mass ratio of the manufactured product to the initial plastic waste sample as reported in the previous studies.[25]

$$Y\% = \left(\frac{\text{Mass of CDs product}}{\text{Mass of plastic waste sampled}}\right) \times 100$$

In this study, when 10 grams of PET-based carbonized material were processed, approximately 4.8 grams of CDs were recovered, yielding 48.16%. The synthesis process is shown in SI Fig S1–S3.

2.4 Characterization of carbon dots

The physicochemical characteristics, surface chemistry, and dispersion behavior of the synthesized carbon dots were analyzed using spectroscopic analysis, particle size analysis, and thermal analysis. A UV–visible spectrophotometer (Shimadzu UV-1800, Japan) was used to measure the absorption spectrum of the CDs between 200 and 800 nm. It was measured in quartz cuvettes with a 1 cm path length, using deionized water as the blank. The photoluminescence (PL) was measured with a spectrofluorometer (Shimadzu RF-6000, Japan). The excitation wavelengths ranged from 300 to 420 nm, and the monitored wavelengths ranged from 350 to 650 nm. The fluorescence performance of the CDs under excitation was analyzed to determine emissive properties arising from surface states. The influence of pH on the fluorescence properties of the CDs was studied by varying the pH of aqueous CD solutions from 2 to 12 using dilute hydrochloric acid (HCl) and sodium hydroxide (NaOH) solutions. Fluorescence stability was compared at a constant excitation wavelength under the same instrumental conditions. A dynamic light scattering analyzer (Malvern Zetasizer Nano ZS, UK) was used to identify the hydrodynamic particle size distribution of the CDs at room temperature. Fourier-transform infrared (FTIR) spectroscopy (Bruker Tensor 27, Germany) over the wavenumber range 4000–400 cm^{-1} was used to characterize the surface functional groups and chemical bonding of the synthesized CDs. X-ray diffraction (XRD) (PANalytical XPert PRO, Netherlands) was used to probe the crystalline architecture of the CDs using Cu Kα radiation (1.5406 Å). Diffraction patterns were measured over a 2θ range of 10–80°, allowing evaluation of the degree of crystallinity and carbonaceous structural order in the CDs. Atomic force microscopy (AFM) was used to investigate the topographical morphology and height of the carbon dot (CD) particles. A dilute CD dispersion was drop-cast onto a cleaned, freshly cleaved mica substrate, allowed to adsorb, gently rinsed with ultrapure water to remove residues, then dried under a stream of nitrogen at room temperature, and finally imaged. Topography was acquired under ambient conditions in tapping mode using an AFM system (Shimadzu WET-SPM 9600, Shimadzu, Tokyo, Japan).

2.5 Photocatalytic application of synthesized CDs

Reactive Black 5 is extensively used in textile dyeing and is commonly detected in colored textile effluents. The azo (–N=N–) linkage and aromatic structure of RB5 make it chemically stable and recalcitrant, which ultimately disturbs the environmental balance.[27] In this regard, RB5 was selected for this study to evaluate the degradation potential of PET-derived carbon dots. All the solutions were prepared by dilution with deionized water (DI), and (0.1 M) HCl/NaOH solutions were used for the adjustment of pH. The stock solution of dye (1000 mg L^{-1}) was prepared in the dark. Then, working solutions were prepared by dilution to the corresponding initial concentration (C_0). The concentrations were evaluated by UV-Vis spectroscopy (Lambda 25, PerkinElmer) at their maximum absorbance (λ_{max}). The absorbance-to-concentration conversion was performed by constructing a calibration curve, as shown in Fig. S4 and Table S1. A batch reactor with a borosilicate beaker was used for photocatalytic experiments, with a working volume of 100 mL and continuous stirring to maintain a homogeneous suspension. A UV-vis lamp (Shimadzu UV-1800, Japan) was used as the irradiation source and maintained at a constant distance throughout all experimental trials to maintain a uniform photon flux.

The designed dosage of CDs (g L^{-1}) was added prior to irradiation. Each experimental trial was stirred in the dark for 30 minutes before irradiation to establish adsorption–desorption equilibrium, which is required to evaluate adsorption-dependent dye removal and to address the overestimation of the photocatalytic ability of the CDs. Photocatalysis started by switching the light source on at time ($t = 0$). After a predetermined time, aliquots were centrifuged and analyzed by UV-vis spectroscopy. The confirmation experiments of the photocatalytic and adsorption potential were performed before the optimization of reaction conditions. The following equation was used to calculate the dye removal % from synthetic wastewater.

$$\text{Dye removal}\% = \frac{C_0 - C_t}{C_0} \times 100$$

The concerned reaction parameters (pH, CD dosage, irradiation/contact time, and initial RB5 concentration) were evaluated, and the BBD model was assessed using replicate center points. The reaction conditions were optimized using Response Surface Methodology (RSM) based on a Box–Behnken design (BBD) with four independent variables: carbon dots dosage (A), initial RB5 concentration (B), pH (C), and irradiation time (D). The experimental design matrix and the corresponding RB5 degradation efficiencies are presented in Table 1.

2.6 Reusability potential of carbon dots

The investigation of the recyclability of the CDs as a photocatalyst for RB5 degradation was carried out under the optimal

Table 1 RSM (BBD) based experimental design for photocatalytic degradation of RB5[a]

Run	*A*: carbon dots dose (g L^{-1})	*B*: dye conc. (mg L^{-1})	*C*: pH	*D*: time (min)	RB5 degradation (%)
1	0.8	30	8	30	68.5
2	0.5	30	5	30	50.2
3	0.8	30	8	120	96.4
4	0.8	30	11	75	87.6
5	0.2	30	11	75	70.8
6	0.5	50	8	30	44.7
7	0.5	30	11	30	55.9
8	0.8	30	5	75	76.1
9	0.5	10	5	75	82.7
10	0.5	30	8	75	88.4
11	0.2	30	8	30	46.8
12	0.2	30	8	120	86.9
13	0.2	10	8	75	84.5
14	0.5	10	8	30	63.8
15	0.8	10	8	75	95.1
16	0.5	30	11	120	92.8
17	0.5	30	8	75	87.6
18	0.5	30	5	120	88.9
19	0.5	10	11	75	88.6
20	0.5	50	11	75	78.9
21	0.5	30	8	75	89.1
22	0.2	50	8	75	66.7
23	0.5	30	8	75	88.0
24	0.5	50	8	120	90.3
25	0.5	10	8	120	95.0
26	0.8	50	8	75	84.2
27	0.5	30	8	75	87.9
28	0.5	50	5	75	74.6
29	0.2	30	5	75	61.9

[a] Experimental data were fitted in a second-order (quadratic) response surface model with 4 factors (*A*, *B*, *C*, and *D*). Time-resolved RSM-predicted data were further quantified to evaluate the kinetics under the optimized conditions and to determine the rate constant and half-life.

photocatalytic conditions for five consecutive runs. At the end of each photocatalytic degradation cycle, the reaction suspension was centrifuged (8000 rpm, 10 min) to separate the photocatalyst from the reaction mixture. The recovered photocatalyst was washed several times with distilled water and ethanol to get rid of the adsorbed dye molecules and intermediate products formed during the degradation process. After washing, it was dried in an oven at 60 °C for 6 h and then reused for the next cycle by adding it to a fresh dye solution with the same concentration. All catalyst reuse experiments were conducted under identical photocatalytic conditions to investigate stability and reusability. The photodegradation efficiency was then determined by UV-Vis study of RB5 before and after exposure to light.

2.7 Statistical analysis

All preliminary calculations were performed in Microsoft Excel, and the graphical presentations were created in Origin Pro 2020. Optimizations and statistical modeling by RSM (BBD) were performed with Stat-ease Design-Expert 360, where the fitting of quadratic regression models and evaluation of ANOVA ($p < 0.05$), including coefficient significance, lack of fit testing, and goodness of fit (R^2, adjusted R^2, and predicted R^2), were supported by actual *vs.* predicted plots and residual diagnostics. Three replicates were measured in all experiments, and the results were reported as mean ± standard deviation (SD).

3 Results and discussion

This study was designed to link the synthesis of carbon dots (CDs) with their structure–property relationships and ultimately apply them to degrade Reactive Black 5 (RB5). The optimal formation of CDs and their main physicochemical characteristics were initially verified by optical (UV-Vis, PL/fluorescence, and pH-dependent fluorescence), chemical (FTIR), structural (XRD), colloidal (DLS), and morphological (AFM) characterization. Based on these results, the performance of the CDs in photocatalytic degradation of RB5 was then interpreted, including the effects of operational variables. Response Surface Methodology (RSM) was used to model and optimize the efficiency of the material, determine the effect of interactions between the factors, and identify optimal conditions to achieve maximum results, assisted by statistical diagnostics and validation experiments.

3.1 Photophysical and optical characteristics of CDs

The UV/Vis absorption spectra of CDs showed typical features of well-structured carbon nanomaterials, aligning with previous findings.[28] The spectrum shown in Fig. 1 features two prominent absorption bands: a sharp peak at 265–270 nm and a broad band at 340–360 nm. The first peak indicates π–π* transitions caused by the aromatic nature of sp^2-hybridized regions in the synthesized carbon dots. The second, broader band corresponds to n–π* transitions, typically associated with carbonyl (C=O) or other oxygen- or nitrogen-based functional groups on the CD surface. These two traits demonstrate significant surface functionalization, which is crucial for explaining CD fluorescence and reactivity. These findings are consistent with the reported literature.[29,30] The UV-vis absorbance data were then converted to the absorption coefficient (ahv), and a plot of $(ahv)^2$ *vs.* photon energy (hv) was drawn as the direct Tauc plot, as shown in Fig. 2. The linear span around the absorption edge was extrapolated to $E_g = 3.14$ eV, indicating permitted electronic changes in the sp^2 domains/surface states of the CDs. This energy range generally facilitates efficient radiative recombination and is expected to exhibit excellent fluorescence.

The photoluminescence characteristics of the CDs were analyzed using fluorescence emission spectroscopy. The excitation wavelengths ranged from 280 to 340 nm, with the fluorescence emission spectra shown in Fig. 3. All wavelengths exhibit emission peaks between 420 and 480 nm, with the strongest at 280 nm. This intense blue fluorescence signals the presence of aromatic and carbonyl groups on the surface, which are known to promote π–π and n–π transitions in carbon dots.[31] The emission peak shifts toward the red region, while

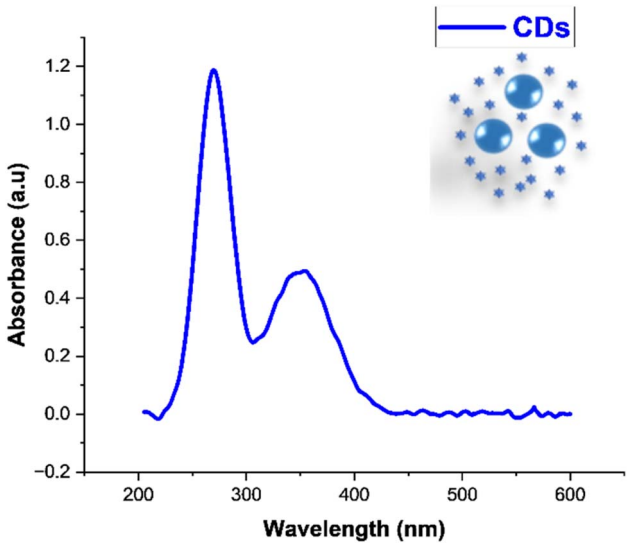

Fig. 1 UV-Vis spectrum of carbon dots showing a strong peak at around 280 nm and a secondary band near 350 nm. The observed transitions suggest π–π* and n–π* electronic transitions of carbon dots.

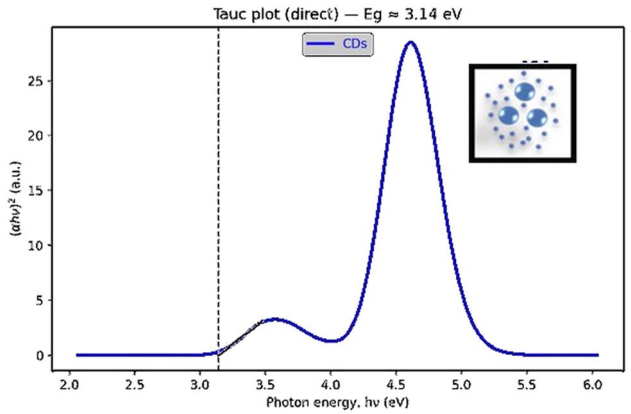

Fig. 2 Direct Tauc plot, $(ahv)^2$ *vs.* photon energy ($h\nu$). The linearity of the absorption edge was estimated from the results, and $(ahv)^2$ was extrapolated to zero.

the reduction in emission intensity can be attributed to multiple surface states and diverse particle sizes that form traps with different emission spectra. A red shift and decreased intensity at an excitation of 340 nm indicate the presence of heterogeneous emissive sites on the CDs. This trend aligns with previous studies showing excitation-dependent blue emission of biomass waste-derived CDs, with a strong signal at 450 nm. The current analysis indicates that emissions are high at low excitation levels, likely due to the polymeric polyethylene terephthalate's extended aromatic-conjugated system. The pH-dependent fluorescence properties of carbon dots (CDs) are an essential feature, especially for environmental monitoring.[32] Fig. 4 shows that the fluorescence intensity of carbon dots varies widely across different pH values, indicating a significant impact of pH on their function. At lower pH values (pH 2–4), the

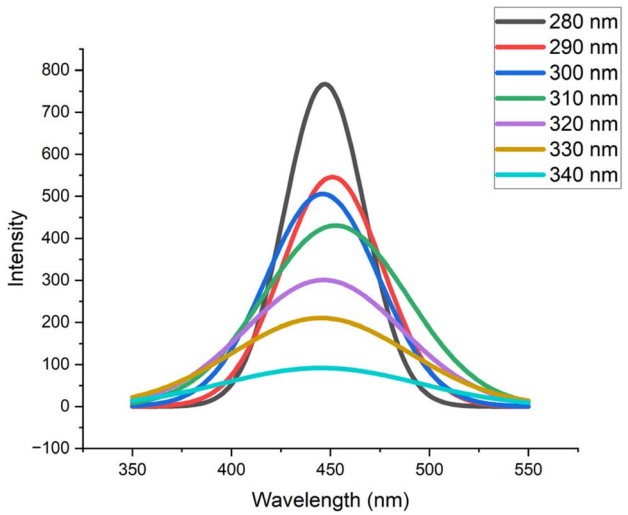

Fig. 3 Fluorescence emission spectra of carbon dots at different excitation wavelengths (280–340 nm).

fluorescence intensity remains relatively low because the surface functional groups, such as –COOH, –OH, and $–NH_2$, become protonated, which disrupts electronic conjugation and quenches fluorescence.[33] As the pH rises from 6 to 12, fluorescence intensity increases accordingly, suggesting deprotonation and stabilization of surface states that support radiative recombination of excited electrons. This observed behavior matches previous research on carbon dots.[34]

3.2 Physicochemical, structural, and morphological analysis

Carbon dots (CDs) are gaining global recognition for their advanced optical, electrical, and biocompatible properties.[35] Fig. 5 illustrates the effect of dynamic light scattering (DLS) on CDs and the distribution of the hydrodynamic diameters of the particles. The percentage of particles, as well as the emergence of a significant peak in the particle size distribution, imply that most of the grown CDs are within a given range of dimensions, indicating homogeneous properties. The presence of only one sharp peak indicates a single dispersant (monodisperse), meaning the dispersants are relatively uniform in size. In contrast, the presence of multiple peaks or a broad distribution suggests polydispersity, as reported earlier.[36] DLS measurements tend to report a hydrodynamic diameter larger than the CD's actual core size. This difference arises from hydration layers and surface functional groups that interact with solvent molecules.[37] The hydrodynamic size of CDs with hydrophilic functional groups, such as –OH and –COOH, is larger due to the solvation effect.[38] A prominent single peak with an estimated size of 5–12 nanometers was observed based on DLS spectra. This indicates that the carbon dots are very tiny and fall within the expected range of quantum-sized nanomaterials. Additionally, the absence of secondary peaks in the graph suggests that there are no large particles or major aggregates in the sample. This implies that the carbon dots are evenly dispersed throughout the solution and that the preparation method effectively prevents particle clumping or uneven size

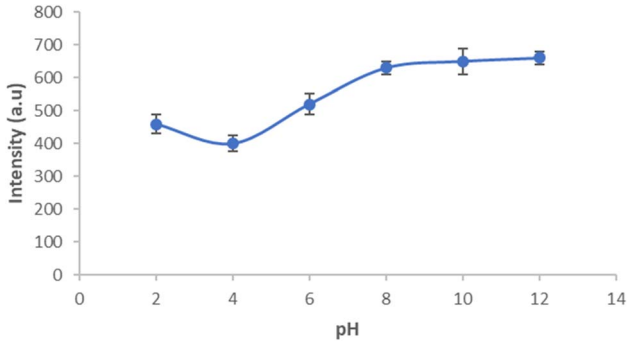

Fig. 4 The pH-dependent variation in the fluorescence emission intensity of carbon dots.

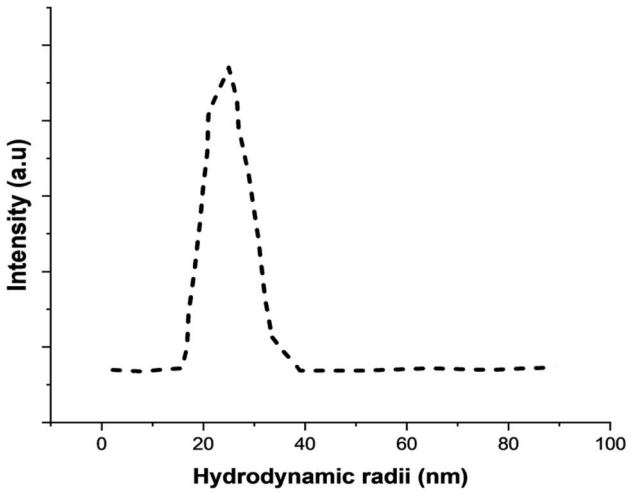

Fig. 5 DLS spectrum of carbon dots indicating a large average particle size distribution with a significant peak at a hydrodynamic radius of 25 nm.

distribution. This monodisperse size distribution is crucial in applications where uniform particle size is critical to performance and stability in biological or environmental systems, such as bioimaging, drug delivery, and photocatalysis.

The FTIR spectrum in Fig. 6 shows prominent peaks corresponding to hydroxyl (–OH), carboxyl (–COOH), carbonyl (C=O), and aromatic C=C groups, indicating successful oxidation and functionalization. The presence of hydroxyl groups was indicated by a broad absorption band at 3200–3500 cm^{-1}, corresponding to O–H stretching vibrations. These hydroxyl groups make the CDs more hydrophilic and soluble in water. The presence of carboxyl groups and those formed during PET oxidation was identified by a strong absorption peak around 1700 cm^{-1}. A signal around 1600 cm^{-1} indicates C=C stretching vibrations, suggesting that aromatic carbon structures in their sp^2 form are still partially preserved in the PET precursor. The stretching of C–O vibrations between 1100 and 1300 cm^{-1} suggests the presence of ether functionalities. The decreased absorption between 600–900 cm^{-1} is related to aromatic C–H bending and is demonstrated by the presence of retained aromatic rings, as indicated by earlier research.[39,40] The

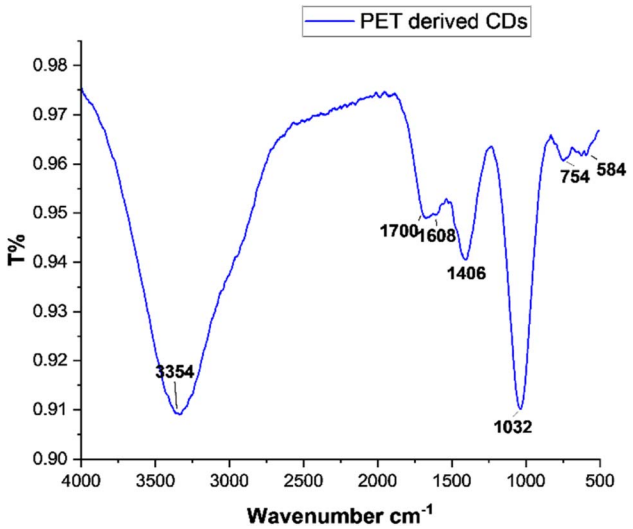

Fig. 6 FTIR spectrum of the synthesized carbon dots.

broad peak of OH/NH in the 3200–3500 cm^{-1} region indicates that the CDs contain many hydrophilic groups, which increase their water solubility and enhance their fluorescence. This has been observed in earlier studies of CDs prepared from biomass like glucose or orange peel, and high hydrophilicity has been closely associated with quantum yield.[41]

PET is inherently aromatic, but when converting to CDs, some of its aromatic nature is preserved, as shown by the C=C skeletal vibrations around 1600 cm^{-1}. Conversely, the loss of ester peaks and the emergence of new functional group signals are major structural changes. This demonstrates that the CDs are entirely new nanostructures formed through a controlled transformation rather than through conventional PET grinding. It has been established that the luminescence behavior of CDs depends on observed FTIR peaks of hydroxyl, amine, carboxyl, and aromatic groups. These groups can facilitate radiative recombination by acting as both electron acceptors and donors. According to the literature, these surface groups play a key role in regulating PL emission. PET-based CDs exhibit FTIR spectra similar to those of CDs derived from natural waste materials such as fruit peels or paper, and their natural polymer backbone confers a slight aromatic character.[42]

The XRD spectrum of Polyethylene Terephthalate (PET) is shown in Fig. 7, with a strong diffraction peak at $2\theta = 16.5$. The origin of this sharp peak represents the semi-crystalline nature of PET, corresponding to the (010) plane of its triclinic crystalline structure. This high crystallinity in the raw PET material produces a sharply defined, intense peak. The lack of extra sharp peaks suggests that there are no multiple crystalline phases, which is common in commercial PET. By contrast, the XRD pattern of the PET-derived carbon dots (CDs) exhibited distinct diffraction peaks at 2θ values of 26.0°, 30.5°, 38.0°, and 43.8°, indicating substantial structural transformation of the original PET material following the three treatment steps. The broadening of these peaks suggests the formation of a nanocrystalline carbon framework, which is characteristic of carbon

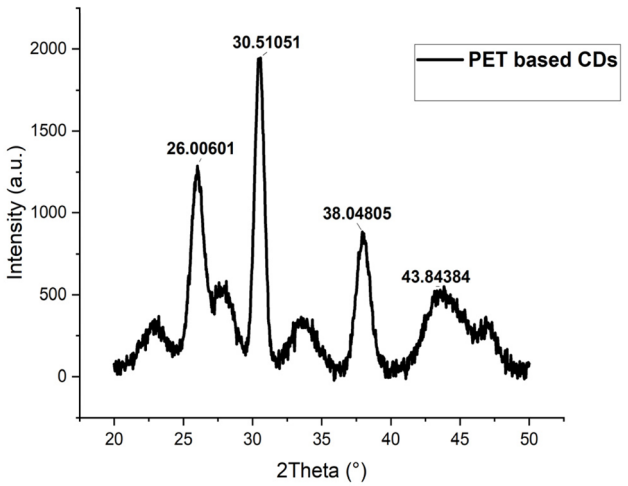

Fig. 7 XRD analysis of PET-derived CDs.

dots synthesized through the thermal decomposition or carbonization of polymeric precursors, as reported in previous studies.[43,44]

The presence of a broad, diffuse peak near $2\theta = 22.6°$ indicates an arrangement of graphitic carbon domains. The peak at 22.6° corresponds to the (002) diffraction peak of graphitic carbon; however, it is notably broader due to the nanoscale roughness of the CDs. The (002) plane of graphitic carbon, which is observed at 26°, indicates that the graphitic or sp^2 hybridized structure of carbon is present in the CD core. The interlayer spacing (d-spacing) in this research was calculated using Bragg's Law and found to be greater than that of crystalline graphite ($d_0 = 3.34$ Å), confirming the presence of disordered graphitic layers, which directly affects their optical and electrical properties. The combination of sp^2 and sp^3 domains creates a structurally diverse carbon network, thereby increasing photoluminescence and enabling variable bandgap behavior. These findings align with the existing literature, which shows that the overall XRD features of carbon dots indicate short-range order and a relatively high degree of disorder when produced from waste polymers, plastic materials, or other polymers.[45,46]

AFM micrographs (10 × 10 μm scan area) clearly demonstrate that the nanoscale carbonaceous domains are dispersed on a smooth matrix. The maximum vertical scale is 30,15 nm as indicated in the 3D image in Fig. 8 and 9, while the topographic scan ($R_a \approx 2.03$ nm; $R_q \approx 3.71$ nm; $R_z \approx 92.45$ nm; $R_p \approx 76.98$ nm; $R_v \approx 15.47$ nm) extracted from the statistical roughness parameters, shows the distribution of nanoscale protrusions across the scanned surface. A homogenous nanostructure is identified with the low average roughness (2 nm),

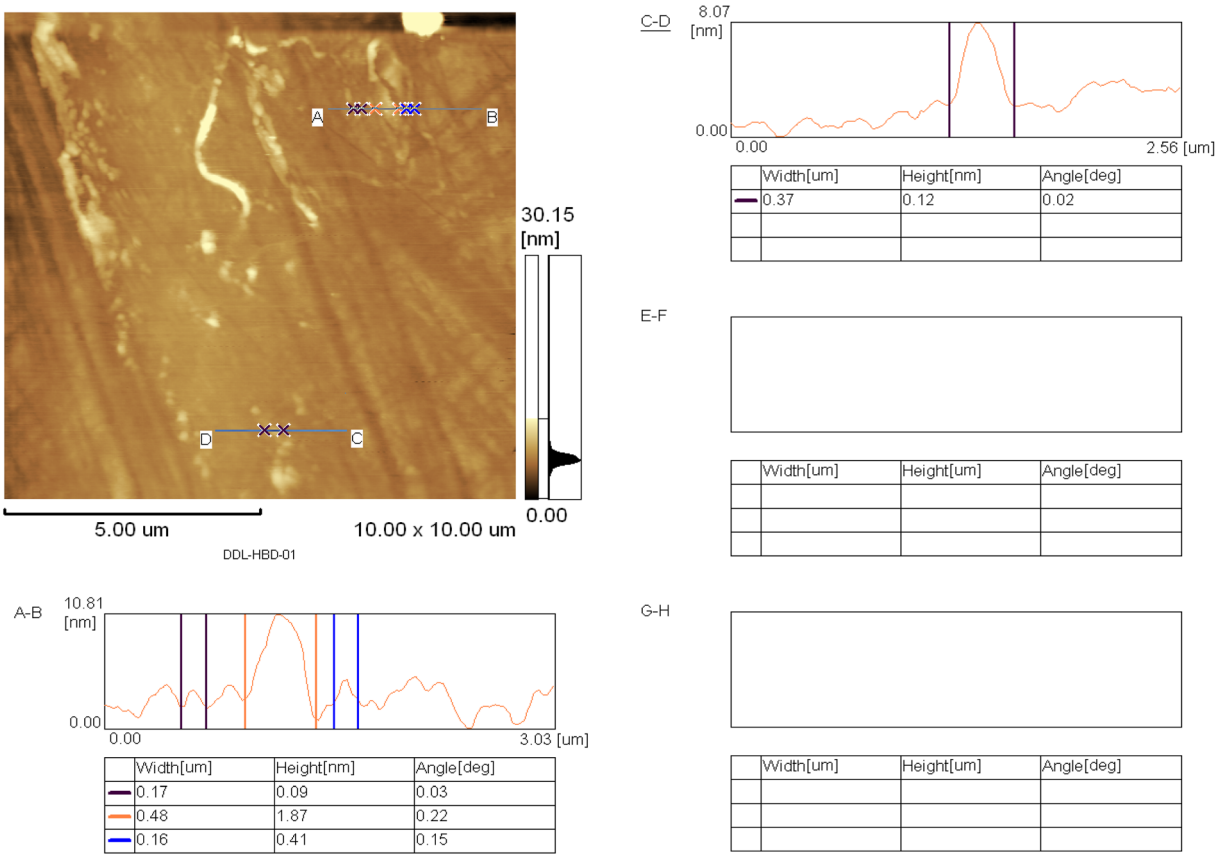

Fig. 8 AFM topography and height profile of carbon dots (CDs). The surface morphology revealed in the 2D AFM height image (scan size 10.00 × 10.00 mm, scale bar 5.00 mm) with the highest and lowest height being 0 and 30.15 nm respectively.

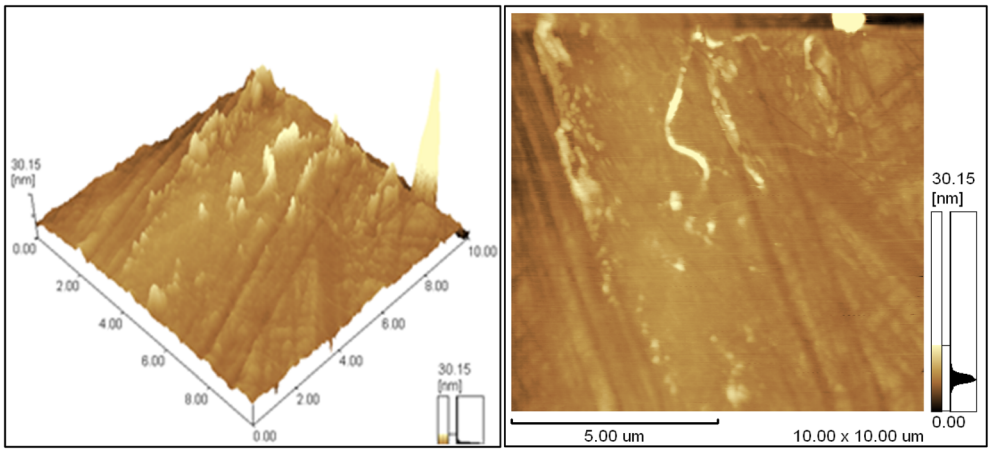

Fig. 9 AFM images of 3D surface topography of CDs deposited over a 10 × 10 μm scan area on the substrate (height scale 0–30.15 nm).

which indicates the formation of nano-range carbon domains consistent with carbon dots, which is further supported by the line profile analysis (A–B) and (C–D). The nanoscale peaks of the height profile reveal sub nanometer to a few (0.4–1.9) nanometers with localized higher protrusions, which indicates the presence of spherical carbon dots with some graphene-like layers. AFM heights commonly fall in the 1–5 nm range with respect to 2–6 nm, embedded in graphene layers, which mostly depend on the synthesis conditions and post-treatment protocols.[47] The elongated and interconnected framework of carbon is induced by calcination followed by hydrothermal treatment and oxidation. Further exfoliation and dispersion of clusters into smaller carbon dots occur with subsequent sonication. A fragmentation-assisted reduction in size is also reported for plastic waste-derived carbon dots in previous studies, where dispersion is improved and particle stacking is reduced by post-treatment sonication.[34] The AFM results of this study show nanoscale profiles having vertical dimensions which are aligned well with the previously reported thickness (1–10 nm) of carbon dots.[27] This indicates that the synthesized carbon dots are not residues of bulk carbon but rather nanoscale dots. The AFM images showed that the surface of carbon dots was rugged and nanostructured with a height difference of 30.15 nm. This provides a greater surface area for the adsorptions of RB5, light absorption and generation of ROS, hence enhancing photocatalytic degradation.

SEM images of a sample taken at different magnifications reveal that the surface morphology is rough, fragmented, solid, and carbonaceous, with small dot-like granular particles randomly dispersed on the surface (Fig. 10). Carbon dots appear to be an irregular, carbon-rich matrix formed post-carbonization, with fine, bright particulate domains attached to the surface at higher magnification (b–d). These particles are aggregated carbon dots on the surface of the carbonaceous material. The aggregation of carbon dots happens because of surface functional groups and extremely small nanoscale dimensions that can lead to aggregation during the drying process. The existence of these dot-like carbonaceous particles on the solid carbonaceous matrix confirms the successful formation of carbon dots.[48]

3.3 Applications of CDs for RB5 degradation

PET-derived carbon dots were studied for their adsorption and photocatalytic degradation potential. The differentiation of both phenomena was analyzed through controlled and confirmatory experiments to understand the actual degradation assisted by CDs. The dye-removal process was further optimized using RSM (Box–Behnken design) to determine the optimal operational window.

3.3.1 Quantification of dark adsorption *vs.* photocatalysis. The dark adsorption equilibrium was established for 30 minutes before each photocatalytic experiment, separating dye removal by adsorption from photocatalysis and preventing overestimation of photocatalytic behavior. In general, increasing the adsorbent dose increases the adsorption rate due to more surface sites and stronger electrostatic and π–π interactions between the adsorbent's functional groups and the dyes.[49] While the adsorption mechanism alone is insufficient for total dye removal, this indicates the presence of a light-mediated pathway.[50,51] The light removal (%) is the sum of the RB5 removal at the conclusion of adsorption + photocatalysis. All runs show a high percentage of light removal, indicating that the additional pathway is another dominant process, activated by light in the presence of adsorption. The maximum light removal of 91.2% was at pH 8, a CD dose of 0.50 g L^{-1}, RB5 = 20 mg L^{-1}, and 65 min, indicating that this condition provides good catalytic activity or good adsorption–reaction coupling, but in-depth optimization can be achieved through statistical methods. In this study, a quadratic RSM model is employed. A pre-optimization baseline summary of the experimental data is presented in Fig. 11, while the corresponding experimental data are provided in Table S2 of the SI.

3.3.2 RSM-based optimization of dye degradation phenomenon. As seen in Fig. 12A, the RB5 degradation efficiency increases significantly with increasing CD dose (0.2–0.8 g L^{-1}) and with increasing pH towards the alkaline pH range. The

optimum degradation is predicted in the high-dose/high-pH area, particularly at 0.8 g L^{-1} CDs and pH 11, at a fixed RB5 concentration of 30 mg L^{-1} and an irradiation time of 75 min. The influence of pH implies that RB5 degradation is also controlled by surface charge, adsorption, and radical formation. The response surface indicates that higher CD doses and basic pH are advantageous for RB5 degradation, as expected for most heterogeneous photocatalytic reactions. Fig. 12B illustrates the increase in RB5 degradation with increasing CD dose and its decrease with increasing initial RB5 concentration. The region with the highest predicted degradation is the high-dose/low-concentration region (0.8 g L^{-1} CDs and 10 mg L^{-1} RB5) at constant pH 7.4 and 75 min. The higher slope along the CD dose axis suggests that the catalyst dose has a greater impact, likely due to the higher surface area and greater ROS formation.

Fig. 12C shows that RB5 degradation increases with the CD dose and light exposure time. The response surface steadily increases with increasing dose and time, indicating a synergistic effect between the two parameters. The response surface suggests that the optimal degradation occurs at 0.8 g L^{-1} CDs and 120 min, with a fixed initial RB5 concentration (26 mg L^{-1}) and pH 7.4. In general, the graph confirms that increasing the catalyst amount and the light exposure time enhances RB5 degradation. The response surface in Fig. 12D shows that the maximum RB5 degradation is predicted at slightly alkaline pH (9–10) and low initial RB5 concentration (10–20 mg L^{-1}). It steadily decreases with increasing RB5 concentration and decreasing pH.

Fig. 12E indicates that RB5 degradation increases with irradiation time from 30 to 120 min, but decreases with increasing initial RB5 concentration from 10 to 50 mg L^{-1}. The highest degradation is obtained at a low dye concentration (10 mg L^{-1}) and a long irradiation time (120 min). However, at higher dye concentrations, around 50 mg L^{-1}, less degradation is observed, even at longer irradiation times. The RB5 degradation increases as the CD dose rises from 0.2 to 0.8 g L^{-1} and exposure time increases from 30 to 120 min, as shown in Fig. 12F. The highest degradation occurs at the highest CD dose (0.8 g L^{-1}) and the longest irradiation time (120 min). To assess the performance of the synthesized CDs relative to previously reported photocatalysts for RB5 degradation, a comparison of degradation

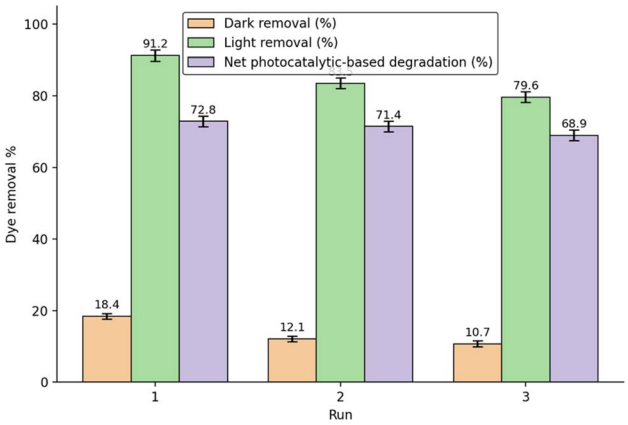

Fig. 11 Analysis of RB5 removal potential *via* dark adsorption, light removal, and net photocatalytic degradation.

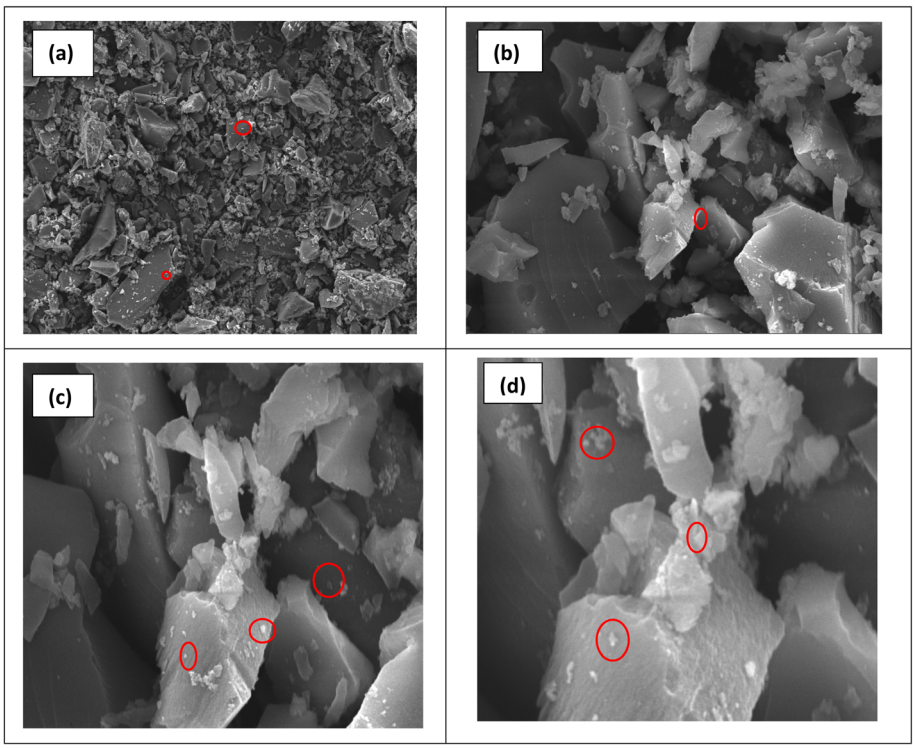

Fig. 10 SEM micrographs of the synthesized carbon dots deposited on the solid carbonaceous surface; (a) 1k magnification, (b) 10k, (c) 30k and (d) 40k.

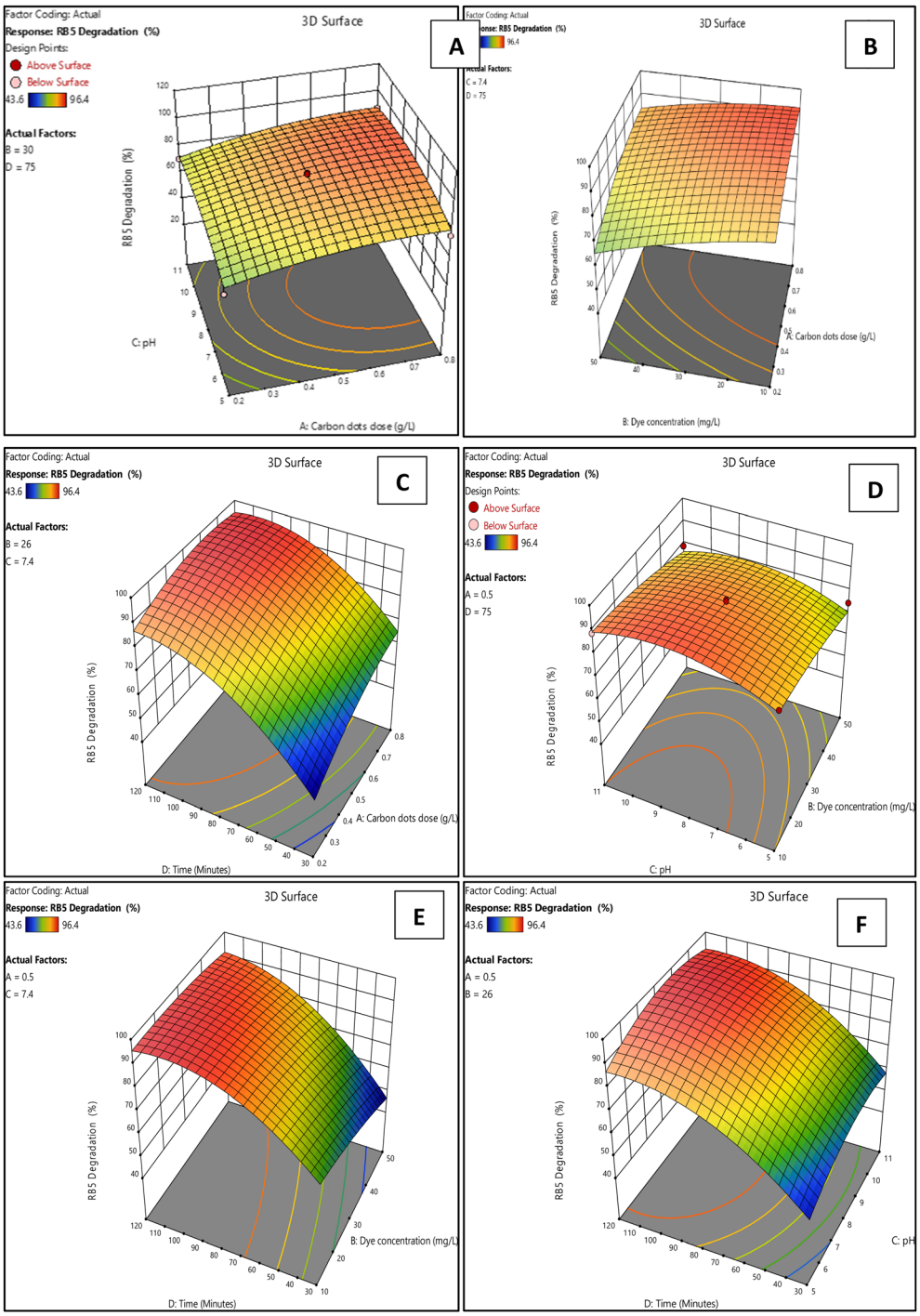

Fig. 12 Three-dimensional response surface plots of the process variables on RBS degradation (%): (A) pH and activated carbon dose, (B) activated carbon dose and dye concentration, (C) time and activated carbon dose, (D) pH and dye concentration, (E) time and dye concentration, and (F) pH and time.

efficiencies under representative operating conditions is presented in Table 2.

As shown in Fig. S5 and S6 of the SI, the relative sensitivity plot and the diagnostic plots for the RB5 degradation model were obtained, which further support the importance of the selected factors as well as the fitted model. The quadratic polynomial equation in terms of coded factors for RB5 degradation is shown as follows:

$$\text{RB5 degradation (\%)} = 88.20 + 7.54A - 5.95B + 3.33C + 18.46D + 1.73AB + 0.7000AC - 3.05AD$$

3.3.3 Integration of RSM findings with pseudo-first-order kinetics. The RB5 degradation was modeled using the outputs in a pseudo-first-order (PFO) kinetic model by transforming the predicted degradation percentage into a fraction of the

Table 2 Comparison of dye-degradation efficiency of the present CD photocatalyst with other photocatalysts

Photocatalyst/system	Dye	Main conditions	Degradation efficiency	References
Carbon dots	RB5	Optimized RSM conditions	96.4 (dark + light)	PET-based carbon dots (current study)
Magnetic nano catalyst	RB5	pH 3, 20 mg L^{-1} RB5, 0.5 g L^{-1} catalyst, 120 min	99.99%	52
nZVI	RB5	Solar irradiation, 120 min	90%	53
ZnO/UV slurry system	RB5	pH 11, UV irradiation	Nearly 99%	54
TiO_2-based photocatalysis	RB5	UV/TiO_2 advanced oxidation process	77%	55

remaining concentration and subsequently into an apparent rate constant.

$$\text{Dye removal}\% = \frac{C_0 - C_t}{C_0} \times 100$$

According to the RSM outcomes the optimized degradation time is 75 minutes with 91.03% degradation.

$$\frac{C_t}{C_0} = 1 - \frac{\text{degradatiom}}{100} = 1 - 91.0375/100 = 0.0896$$

$$\ln\frac{C_t}{C_0} = \ln\left(1 \Big/ \frac{C_t}{C_0}\right) = \ln\ 1/0.896 = 2.4121$$

With respect to the pseudo-first-order model:

$$\ln\frac{C_t}{C_0} = k_{\text{app}} \times t$$

$$k_{\text{app}} = \frac{\ln\left(\frac{C_t}{C_0}\right)}{t} = \frac{2.4121}{75} = 0.03216\ \text{min}^{-1}$$

half-life:

$$t_{1/2} = \ln(2)/k_{\text{app}} = 0.6931/0.03216 = 21.6\ \text{min}$$

RSM predicted ($t = 75$ minutes) points were plotted to evaluate the kinetic trend of the data. The tabular data are presented in the supplementary file as Table S2, while the plots described in Fig. 13 demonstrate that dye degradation under the RSM predicted optimized conditions ($t = 75$ min) follows a pseudo-first-order reaction whereby the higher the degradation (%), the higher the apparent rate constant (k_{app}) and, consequently, the faster the reaction under the same conditions. The half-life ($t_{1/2}$) is also determined using the pseudo-first-order model, which decreases with increasing dye degradation, falling between approximately 60 and 20 minutes. In general, the greater the degradation, the larger the k_{app}, and the shorter the $t_{1/2}$, indicating better kinetic performance and faster dye degradation. The pseudo-first-order kinetic parameters and RSM model summary are presented in Tables S3 and S4 of the SI.

3.3.4 RSM predicted data: statistical evaluation. The ANOVA results revealed that the quadratic RSM model used to predict RB5 degradation was significant ($F = 46.63$, $p < 0.0001$), and model summary tables are given in the SI as Table S6. The goodness of fit of the model was high ($R^2 = 0.9790$), and the adjusted $R_2 = 0.9580$ and the predicted $R^2 = 0.8799$. The model

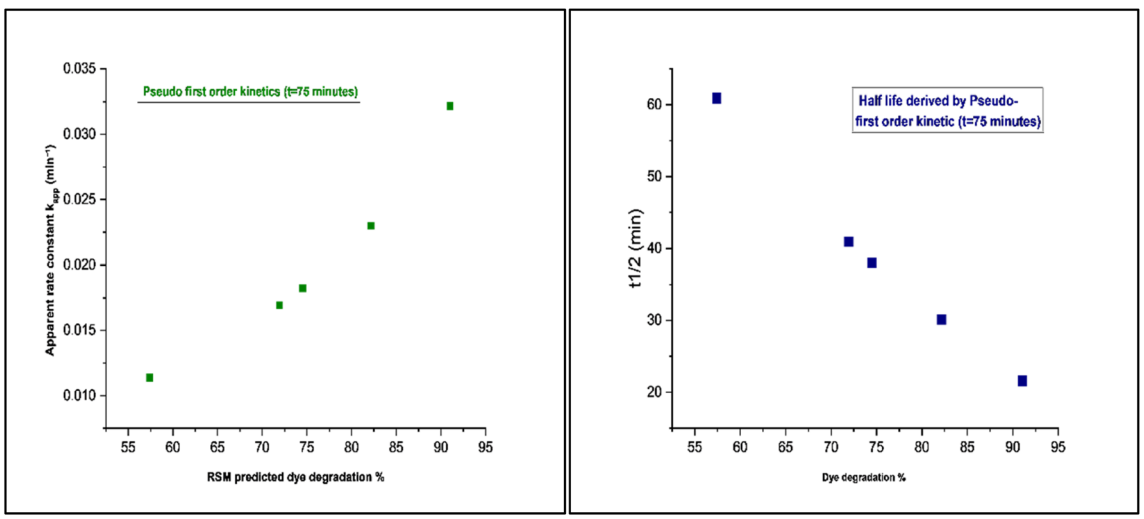

Fig. 13 Pseudo-first-order kinetic trend of RB5 degradation for 75 min: fluctuation of k_{app} (left) and $t_{1/2}$ (right) with predicted dye removal (%).

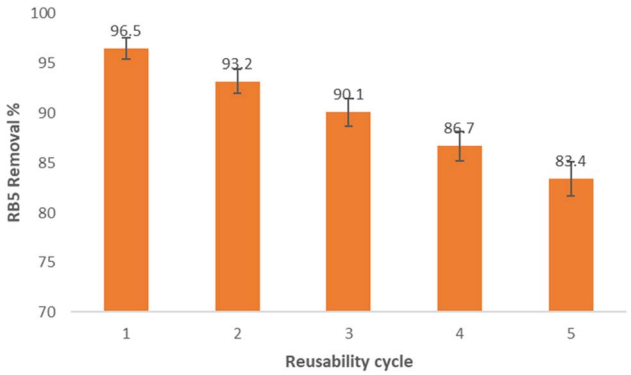

Fig. 14 Reusability of CDs for five consecutive cycles.

accuracy was reasonable, as shown by the low CV (3.98) and high Precision (23.38). There were significant linear effects of the dose of carbon dots, concentration of dye used, pH and time (A, B, C and D respectively) and time (D) influenced the response the most (F-value = 2.6). Among the interaction terms, only BD turned out to be significant ($p = 0.0262$), which indicates the joint effect of dye concentration and time. The quadratic terms A^2 ($p = 0.0018$), C^2 ($p < 0.0001$) and D^2 ($p < 0.0001$) were significant, which indicated that the response surface was curvilinear. The significance of the lack-of-fit test ($p = 0.0014$) was high; thus, to test the model's assumptions, diagnostic plots were used to assess whether the residuals were randomly distributed.

3.4 Reusability potential of carbon dots

The reusability of the CD photocatalyst showed that good photocatalytic degradation of RB5 could be achieved after five uses. The degradation efficiency slightly decreased with an increasing number of cycles, due to surface fouling, small catalyst loss during the recovery process, or blockage of active sites by intermediate products.[56] The maintained efficiency after 5 cycles confirms satisfactory stability and reusability of CDs for the photocatalytic degradation of RB5 as shown in Fig. 14. The slight decrease in photocatalytic activity after repeated runs could be attributed to a small loss of catalyst during recovery and washing steps and partial coverage of active sites by adsorbed dye molecules or degradation intermediates, leaving fewer active sites and less surface area for next cycles.[57]

4 Conclusion

This research has shown the effective recycling of waste PET bottles to carbon dots (CDs) and their subsequent use as photocatalysts for Reactive Black 5 (RB5) dye removal. The CDs exhibited desirable optical and surface characteristics with a typical UV-vis absorption spectrum, blue photoluminescence emission, oxygen-/nitrogen-containing functional groups, nanoscale size and a rough surface, facilitating dye interaction and photocatalytic activity. The RSM model identified optimal conditions for the dark adsorption/light photocatalytic process, which resulted in 96.5% removal of RB5. The RSM model demonstrated good predictability and revealed the significance of CD dose, initial dye concentration, pH, and UV irradiation time for degradation efficiency. The CDs were also found to be stable for recycling, with good performance over five cycles. In summary, this study offers an easy, eco-friendly, and waste-to-value approach for the sustainable treatment of dye-polluted water.

Author contributions

Seemab Javed was responsible for the conceptualization, methodology, investigation, data curation, and initial draft preparation. Shahzad Ali Shahid Chatha and Aman Ullah supervised the study, guiding its direction and methodology, and assisted with editing and manuscript review. Shafqat Ali oversaw the work and provided crucial input to review and improve the project analysis.

Conflicts of interest

There is no conflicts of interest.

Data availability

The data supporting the findings of this study are available from the corresponding author upon reasonable request.

Supplementary information (SI) is available. See DOI: https://doi.org/10.1039/d6va00121a.

Acknowledgements

The author gratefully acknowledges the guidance and support of Dr Aman Ullah, Dr Shahzad Ali Shahid Chatha, and Dr Shafaqat throughout the research process. Their supervision and feedback were crucial to this study. Additionally, the authors appreciate the support of the Department of Chemistry and the Department of Environmental Science at Government College University, Faisalabad, and the Department of Agriculture, Food and Environmental Science, University of Alberta, Canada, for providing laboratory facilities and technical assistance in synthesizing and characterizing carbon dots from PET waste and their photocatalytic application.

References

1 A. M. Abdelfatah, M. Hosny, A. S. Elbay, N. El-Maghrabi and M. Fawzy, From Waste to Worth: Upcycling Plastic into High-Value Carbon-Based Nanomaterials, *Polymers*, 2024, **17**, 63.
2 M. Anwar, M. E. Konnova and S. Dastgir, Circular Plastic Economy for Sustainable Development: Current Advances and Future perspectives, *RSC Sustain.*, 2025, **3**, 3724–3840.
3 R. Vanaraj, S. M. Suresh Kumar, S. C. Kim and M. Santhamoorthy, A review on sustainable upcycling of plastic waste through depolymerization into high-value monomer, *Processes*, 2025, **13**, 2431.
4 J. Mehta, N. Dilbaghi, A. Deep, F. I. Hai, A. A. Hassan, A. Kaushik and S. Kumar, Plastic waste upcycling into

carbon nanomaterials in circular economy: Synthesis, applications, and environmental aspects, *Carbon*, 2025, **234**, 119969.

5 X. Mu, Y. Li, X. Liu, C. Ma, H. Jiang, J. Zhu, X. Chen, T. Tang and E. Mijowska, Controllable carbonization of plastic waste into three-dimensional porous carbon nanosheets by combined catalyst for high performance capacitor, *Nanomaterials*, 2020, **10**, 1097.

6 Y. Wu, G. Ma, A. Zhang, W. Gu, J. Wei and R. Wang, Preparation of carbon dots with ultrahigh fluorescence quantum yield based on PET waste, *ACS Omega*, 2022, **7**, 38037–38044.

7 W. Gu, Z. Dong, A. Zhang, T. Ma, Q. Hu, J. Wei and R. Wang, Functionalization of PET with carbon dots as copolymerizable flame retardants for the excellent smoke suppressants and mechanical properties, *Polym. Degrad. Stab.*, 2022, **195**, 109766.

8 S. Chaudhary, M. Kumari, P. Chauhan and G. R. Chaudhary, Upcycling of plastic waste into fluorescent carbon dots: An environmentally viable transformation to biocompatible C-dots with potential prospective in analytical applications, *Waste Manage.*, 2021, **120**, 675–686.

9 C. Ma, G. Jin, P. He, C. Tang, L. Bing, B. Liu, H. Huang, Y. Fan, R. Wang and J. Wei, Optimization of preparation technology for PET-based Carbon Dots by response surface method and its application, *J. Fluoresc.*, 2025, **35**, 6875–6885.

10 N. Eldomiaty, E. Elbayoumy, M. M. Aboelnga and M. R. Mostafa, Repurposing waste plastic into a sustainable adsorbent for removing synthetic dye: experimental, optimization and theoretical modeling, *RSC Adv.*, 2026, **16**, 1008–1029.

11 Y. Jiang, X. Zhang, L. Xiao, R. Yan, J. Xin, C. Yin, Y. Jia, Y. Zhao, C. Xiao and Z. Zhang, Preparation of dual-emission polyurethane/carbon dots thermoresponsive composite films for colorimetric temperature sensing, *Carbon*, 2020, **163**, 26–33.

12 Y. Iqbal, S. A. Shahid Chatha, I. Ahmed, K. Shahzad, M. Y. Siddique and U. Anwar, Moringa Gum-derived Polymeric Carbon Dots for Antimicrobial Activity, *Bioresources*, 2025, **20**(2), 4479–4494.

13 Y. Zhou, W. Zhang and R. M. Leblanc, Structure–property–activity relationships in carbon dots, *J. Phys. Chem. B*, 2022, **126**, 10777–10796.

14 M. M. Islam, A. R. Aidid, J. N. Mohshin, H. Mondal, S. Ganguli and A. K. Chakraborty, A critical review on textile dye-containing wastewater: Ecotoxicity, health risks, and remediation strategies for environmental safety, *Clean. Chem. Eng.*, 2025, **11**, 100165.

15 M. K. A. Elnabi, M. A. Ghazy, S. S. Ali, M. Eltarahony and A. Nassrallah, Efficient biodegradation and detoxification of reactive black 5 using a newly constructed bacterial consortium, *Microb. Cell Factories*, 2025, **24**, 154.

16 S. Sadiq, S. A. S. Chatha, S. Ali, M. Shahid and P. K. Sarker, Microwave assisted synthesis of fly ash based zeolites for degradation of reactive blue 19 dye from wastewater, *Sci. Rep.*, 2025, **15**, 16028.

17 H. A. Kiwaan, R. M. Basal, M. M. Aboelnga and M. R. Mostafa, Efficient photo-assisted degradation of wastewater dyes using CdS nanoparticles confined in porous G-C3N4/SiO2 composites, *J. Mol. Liq.*, 2023, **391**, 123301.

18 M. Magdy, M. M. Aboelnga and E. Elbayoumy, Sustainable removal of brilliant green dye from aqueous media using a calcium alginate–polydopamine bio-composite: process optimization and adsorption mechanism, *Mater. Adv.*, 2026, **7**, 2785–2802.

19 S. S. Makgato, Analysis of municipal solid waste in Soweto, Johannesburg Municipality, South Africa: Implications for sustainable waste management practices, *Chem. Eng. Trans.*, 2024, **109**, 37–42.

20 A. M. Parambil and P. Rajamani, Carbon dots: a promising path towards environmental sustainability, *Environ. Sci. Adv.*, 2024, **3**, 1513–1523.

21 A. D. Ambaye, T. G. Kebede, N. Raleie, S. Dube, M. Mathe, M. M. Nindi, S. Makgato and T. Mokrani, Recent advances in carbon dot-driven nanomaterials for photoelectrochemical-based degradation of contaminants: A Review, *Int. J. Electrochem. Sci.*, 2026, 101297.

22 K. F. Kayani, S. J. Mohammed, M. S. Mustafa and S. B. Aziz, Dyes and their toxicity: removal from wastewater using carbon dots/metal oxides as hybrid materials: a review, *Mater. Adv.*, 2025, **6**, 5391–5409.

23 L. Buenaño, E. Ali, A. Jafer, S. H. Zaki, F. J. Hammady, S. B. Khayoun Alsaadi, M. M. Karim, M. F. Ramadan, A. A. Omran and A. Alawadi, Optimization by Box–Behnken design for environmental contaminants removal using magnetic nanocomposite, *Sci. Rep.*, 2024, **14**, 6950.

24 M. Hussain, A. Abbas, T. Ahmad, S. Ullah, S. Chatha and T. Shifa, Na-alginate coated waste banana-derived biochar composite for heavy metals removal and parametric optimization using RSM-CCD model, *Int. J. Environ. Sci. Technol.*, 2026, **23**, 159.

25 X. Zhou, J. Deng, Z. Li, Y. Cheng, J. Zhou, M. Jiang and W. Dong, One-Pot Synthesis of Multicolor Carbon Dots from PET Plastic Waste for White Light-Emitting Diodes, *ACS Sustain. Chem. Eng.*, 2024, **12**, 16592–16602.

26 I.-H. Tsai, J.-T. Li and C.-W. Chang, Effects of sonication and hydrothermal treatments on the optical and chemical properties of carbon dots, *ACS Omega*, 2021, **6**, 14174–14181.

27 L. Cao, J. Li, Y. Song, S. Cong, H. Wang and M. Tan, Molecular interaction of fluorescent carbon dots from mature vinegar with human hemoglobin: Insights from spectroscopy, thermodynamics and AFM, *Int. J. Biol. Macromol.*, 2021, **167**, 415–422.

28 D.-K. Lee, S. Jeon, J. Jeong, K. S. Song and W.-S. Cho, Carbon nanomaterial-derived lung burden analysis using UV-Vis spectrophotometry and proteinase K digestion, *Part. Fibre Toxicol.*, 2020, **17**, 43.

29 Y. Wu, R. Wang, W. Xie, G. Ma, A. Zhang, B. Liu, H. Huang, L. Gao, M. Qu and Y. Wei, Solvent-thermal preparation of sulfur and nitrogen-doped carbon dots with PET waste as precursor and application in light-blocking film, *J. Nanopart. Res.*, 2023, **25**, 18.

30 J. Jiang, G. Ye, Z. Wang, Y. Lu, J. Chen and K. Matyjaszewski, Heteroatom-Doped Carbon Dots (CDs) as a Class of Metal-Free Photocatalysts for PET-RAFT Polymerization under Visible Light and Sunlight, *Angew. Chem.*, 2018, **130**, 12213–12218.
31 P. Roy, P.-C. Chen, A. P. Periasamy, Y.-N. Chen and H.-T. Chang, Photoluminescent carbon nanodots: synthesis, physicochemical properties and analytical applications, *Mater. Today*, 2015, **18**, 447–458.
32 W. K. Szapoczka, A. L. Truskewycz, T. Skodvin, B. Holst and P. J. Thomas, Fluorescence intensity and fluorescence lifetime measurements of various carbon dots as a function of pH, *Sci. Rep.*, 2023, **13**, 10660.
33 C. Liu, F. Zhang, J. Hu, W. Gao and M. Zhang, A mini review on pH-sensitive photoluminescence in carbon nanodots, *Front. Chem.*, 2021, **8**, 605028.
34 P. K. Arpita, N. Kataria, N. Narwal, S. Kumar, R. Kumar, K. S. Khoo and P. L. Show, Plastic waste-derived carbon dots: insights of recycling valuable materials towards environmental sustainability, *Curr. Pollut. Rep.*, 2023, **9**, 433–453.
35 Z. Chen, Y. Liu and Z. Kang, Diversity and tailorability of photoelectrochemical properties of carbon dots, *Acc. Chem. Res.*, 2022, **55**, 3110–3124.
36 N. A. Lynd, A. J. Meuler and M. A. Hillmyer, Polydispersity and block copolymer self-assembly, *Prog. Polym. Sci.*, 2008, **33**, 875–893.
37 Z. Jia, J. Li, L. Gao, D. Yang and A. Kanaev, Dynamic light scattering: a powerful tool for in situ nanoparticle sizing, *Colloid Interface Sci.*, 2023, **7**, 15.
38 J. Rodriguez-Loya, M. Lerma and J. L. Gardea-Torresdey, Dynamic light scattering and its application to control nanoparticle aggregation in colloidal systems: a review, *Micromachines*, 2023, **15**, 24.
39 M. Egorova, A. Tomskaya and S. A. Smagulova, Optical properties of carbon dots synthesized by the hydrothermal method, *Materials*, 2023, **16**, 4018.
40 C. M. Singaravelu, X. Deschanels, C. Rey and J. Causse, Investigation on Fluorescence Origin and Spectral Heterogeneity in Carbon Dots: A Dynamic Perspective, *ChemPhotoChem*, 2024, **8**, e202400044.
41 P. F. Andrade, G. Nakazato and N. Durán, *J. Phys.: Conf. Ser.*, 2017, **838**, 012028.
42 J. Ren, F. Weber, F. Weigert, Y. Wang, S. Choudhury, J. Xiao, I. Lauermann, U. Resch-Genger, A. Bande and T. Petit, Influence of surface chemistry on optical, chemical and electronic properties of blue luminescent carbon dots, *Nanoscale*, 2019, **11**, 2056–2064.
43 K. J. Mintz, M. Bartoli, M. Rovere, Y. Zhou, S. D. Hettiarachchi, S. Paudyal, J. Chen, J. B. Domena, P. Y. Liyanage and R. Sampson, A deep investigation into the structure of carbon dots, *Carbon*, 2021, **173**, 433–447.
44 A. Kelarakis, From highly graphitic to amorphous carbon dots: A critical review, *MRS Energy Sustain.*, 2014, **1**, E2.
45 P. Ma, J. Zuo, Z. Li, D. Xiao, H. Wu, Y. Zhang and A. Dong, Application progress of green carbon dots in analysis and detection, *Part. Part. Syst. Char.*, 2022, **39**, 2200104.
46 Y. Chen, X. Zhu, H. Liu and B. Sun, Synergistic PET/IFE-driven fluorescence-phosphorescence dual signal quenching in RTP CDs sensor for sensitive thiram monitoring in food safety, *Microchim. Acta*, 2025, **192**, 1–10.
47 M. Aasadnia, M. Mehrpooya and B. Ghorbani, A novel integrated structure for hydrogen purification using the cryogenic method, *J. Clean. Prod.*, 2021, **278**, 123872.
48 B. D. Mansuriya and Z. Altintas, Carbon dots: classification, properties, synthesis, characterization, and applications in health care—an updated review (2018–2021), *Nanomaterials*, 2021, **11**, 2525.
49 J. Feng, X. Ran, L. Wang, B. Xiao, L. Lei, J. Zhu, Z. Liu, X. Xi, G. Feng and Z. Dai, The synergistic effect of adsorption-photocatalysis for removal of organic pollutants on mesoporous Cu2V2O7/Cu3V2O8/g-C3N4 heterojunction, *Int. J. Mol. Sci.*, 2022, **23**, 14264.
50 S. Tak, S. Grewal, S. Shreya, P. Phogat, D. Manisha, R. Jha and S. Singh, Mechanistic insights and emerging trends in photocatalytic dye degradation for wastewater treatment, *Chem. Eng. Technol.*, 2024, **47**, e202400142.
51 S. Khan, T. Noor, N. Iqbal and L. Yaqoob, Photocatalytic dye degradation from textile wastewater: a review, *ACS Omega*, 2024, **9**, 21751–21767.
52 M. Mohammadi-Galangash, S.-K. Mousavi and M. Shirzad-Siboni, Photocatalytic degradation of reactive black 5 from synthetic and real wastewater under visible light with TiO2 coated PET photocatalysts, *Sci. Rep.*, 2025, **15**, 14314.
53 H. Nassehinia, H. Rahmani, K. Rahmani and A. Rahmani, Solar photocatalytic degradation of Reactive Black 5: by-products, bio-toxicity, and kinetic study, *Desalination Water Treat.*, 2020, **206**, 385–395.
54 S. Laohaprapanon, J. Matahum, L. Tayo and S.-J. You, Photodegradation of reactive black 5 in a ZnO/UV slurry membrane reactor, *J. Taiwan Inst. Chem. Eng.*, 2015, **49**, 136–141.
55 E. Kusvuran, S. Irmak, H. I. Yavuz, A. Samil and O. Erbatur, Comparison of the treatment methods efficiency for decolorization and mineralization of Reactive Black 5 azo dye, *J. Hazard. Mater.*, 2005, **119**, 109–116.
56 K. J. Amaya-Galván, K. J. Ramírez-Escárcega, F. L. Zaruma-Torres, F. d. J. Silerio-Vazquez and J. B. Proal-Nájera, Pharmaceutical pollutants in water: Carbon nanotube–photocatalyst composites as a path forward, *J. Environ. Chem. Eng.*, 2025, **13**, 115086.
57 P. Gharbani, A. Mehrizad and S. A. Mosavi, Optimization, kinetics and thermodynamics studies for photocatalytic degradation of Methylene Blue using cadmium selenide nanoparticles, *npj Clean Water*, 2022, **5**, 34.

